# scientific reports



# **OPEN** Evaluation of condensation silicone dental impression materials modified with diatomaceous Earth and zinc oxide fillers

Mohsen Fakoori<sup>1</sup>, Saeed Hesaraki<sup>1⊠</sup>, Nader Nezafati<sup>1</sup> & Majid ghiass<sup>2</sup>

Condensation silicones are widely used for dental impressions due to their handling ease and affordability but have limitations like shrinkage, suboptimal rheology, and bacterial contamination risk. This study investigated the effects of incorporating microsized diatomaceous earth (DE) and zinc oxide (ZnO) on the physical, mechanical, rheological, and antibacterial properties of condensation silicone dental impression material. DE/ZnO powders were ball-milled with silica and calcium carbonate, then mixed with hydroxy-terminated polydimethylsiloxane and tetraethyl orthosilicate. The resulting pastes, including a control, were evaluated. Microstructural analysis was conducted via SEM, EDAX, and XRD. SEM/EDAX confirmed filler incorporation: dispersed needle-like ZnO and localized DE aggregates in the silicone matrix. XRD verified ZnO crystalline wurtzite structure and DE cristobalite phase. Incorporating of DE/ZnO extended the setting time and improved the flowability. Compared to the control, ZnO incorporation significantly enhanced dimensional stability, extended working time, slightly decreased hardness, exhibited a lower elastic modulus with significantly higher elongation, and moderately improved wettability. DE incorporation shortened working time, did not improve dimensional stability, slightly decreased hardness, showed similar elastic modulus to the control but with higher elongation, and significantly improved wettability. Antibacterial tests against E. coli and S. mutans revealed significant activity for the ZnO-containing samples but no effects for the DE-containing samples. No significant differences were found in the mixing times among the samples. Results show distinct filler roles: ZnO improves functional properties (stability, antibacterial) and DE modifies surface characteristics (wettability), highlighting potential for targeted property tailoring through filler choice.

Keywords Condensation silicone, Dental materials, Diatomaceous Earth, Impression material, Zinc oxide

The accuracy of dental impressions is crucial in modern dentistry for achieving optimal results in prosthodontics, restorative dentistry, and orthodontics<sup>1,2</sup>. These impressions form the basis of a wide range of dental prostheses such as inlays, onlays, crowns, bridges, and orthodontic appliances<sup>3</sup>. The fidelity of the impression directly affects the fit, function, and longevity of these restorations and, therefore, has implications for patient satisfaction and oral health. Traditionally, impression materials evolved from rigid materials like plaster to elastic materials such as agar and alginate, which had limitations in accuracy and detail capture<sup>4,5</sup>. The discovery of elastomeric impression materials led to revolutionary changes in dentistry, where improved accuracy, dimensional stability, and reproduction of fine anatomical detail could be achieved<sup>6,7</sup>. Among elastomers, condensation silicones, a type of polysiloxane characterized by a setting reaction that releases a byproduct, have gained widespread use owing to their favorable characteristics, such as easy handling, excellent elastic recovery, and relatively good dimensional stability<sup>8-10</sup>. These materials usually consist of a base polymer, typically a polydimethylsiloxane with terminal hydroxyl groups, and a cross-linking agent, which is more often an alkoxysilane (tetraethyl orthosilicate, TEOS), in addition to fillers and catalysts, to properly control the setting reaction and final properties<sup>11–13</sup>.

Despite their advantages, condensation silicones possess inherent disadvantages. One significant disadvantage is inherent; the very mechanism of polymerization involves the emission of a byproduct, in most cases ethanol. This volatile byproduct can cause changes in dimensions and a subsequent decrease in accuracy<sup>14</sup>. Another

<sup>1</sup>Biomaterials Group, Department of Nanotechnology and Advanced Materials, Materials and Energy Research Center, Alborz, Iran. <sup>2</sup>Department of Novel Drug Delivery Systems, Iran Polymer and Petrochemical Institute (IPPI), Tehran, Iran. <sup>™</sup>email: S-hesaraki@merc.ac.ir

challenge is achieving optimal rheological and mechanical properties along with satisfactory wettability for condensation silicone impression materials. Addressing these limitations is crucial to improve the performance and clinical applicability of these materials<sup>15</sup>. Furthermore, disinfection protocols, while necessary, can also introduce dimensional changes, compounding accuracy issues<sup>16</sup>. In this respect, modifications have been carried out in the formulation of impression silicones, mainly by the addition of various types of fillers<sup>17,18</sup>. Fillers can have a significant effect on the physical, mechanical and rheological properties of the impression material.

Diatomaceous earth (DE), a biogenic sedimentary rock primarily composed of fossilized diatom remains, is a promising biomaterial with potential applications in dental materials  $^{19-21}$ . The unique physicochemical properties of DE stem from its high silica content (80–90% SiO2) coupled with the presence of other metal oxides, such as alumina (Al<sub>2</sub>O<sub>3</sub>) and iron oxide (Fe2O3)<sup>22</sup>. The intricate, porous structure of DE, resulting from the diverse shapes and sizes of diatom frustules, contributes to its high surface area, low density, and chemical inertness<sup>23</sup>. These characteristics, along with its inherent biocompatibility, have led to its widespread use in various fields, including filtration, absorption and drug delivery  $^{21,24,25}$ . The versatility of DE extends to its use as a filler in dental impression materials, such as alginates, which are widely used in dentistry for creating diagnostic and working casts<sup>26</sup>.

Zinc oxide (ZnO) is a versatile inorganic compound that has established applications in a variety of dental materials, and its potential applications in impression materials are an area of growing interest<sup>27,28</sup>. ZnO is valued for its biocompatibility, affordability, ability to impart antimicrobial properties, and potential to enhance mechanical properties<sup>29–32</sup>. In restorative dentistry, ZnO is added to resin composites, glass ionomer cements, and dental amalgams to enhance their mechanical properties, durability, and antimicrobial activity<sup>33</sup>. The potential benefits of incorporating ZnO into impression materials, however, have received less attention.

To date, research exploring the impact of fillers on condensation silicone impression materials has been limited. This study investigates the effects of two distinct filler types (DE and ZnO) on a comprehensive suite of clinically relevant properties of these materials. Specifically, the mixing time, working time, setting time, rheological behavior, dimensional stability, tensile properties, hardness, wettability, and antibacterial activity are examined. This investigation seeks to provide valuable insights into how these fillers might improve the performance and clinical utility of condensation silicone impression materials.

# Materials and methods Sample Preparation

The pastes were prepared using the following materials: the base polymer, hydroxyl-terminated polydimethylsiloxane (PDMS-OH) (viscosity: 3500 cSt, density: 0.97 g/cm³, Sigma-Aldrich˚, Germany); fillers including silica (SiO<sub>2</sub>) (average particle size: 25 μm, density: 2.65 g/cm³, Neutron˚ Pharmaceutical Chemical Company, Iran), calcium carbonate (CaCO<sub>3</sub>) (density: 2.71 g/cm³, Sigma-Aldrich˚, Germany), diatomaceous earth (DE) (particle size < 20 μm, density: 2.30 g/cm³, Neutron˚ Pharmaceutical Chemical Company, Iran), and zinc oxide (ZnO) (particle size: ~1 μm, density: 5.61 g/cm³, Neutron˚ Pharmaceutical Chemical Company, Iran); the crosslinking agent, tetraethyl orthosilicate (TEOS) (density: 0.93 g/cm³, Sigma-Aldrich˚, Germany); absolute ethanol (99.99%, Sigma-Aldrich˚, Germany); and a commercial condensation silicone activator (Speedex Universal Activator, Coltène, Switzerland). A series of condensation silicone base pastes were formulated to investigate the effects of DE and ZnO on the physical, mechanical, rheological, and antibacterial properties of dental impression materials. The detailed compositions of these base pastes are presented in Table 1.

A control paste (Base Paste) was prepared using a mixture of SiO<sub>2</sub> and CaCO<sub>3</sub> fillers within the PDMS-OH matrix, along with TEOS as a crosslinking agent. It is crucial to note that plain hydroxyl-terminated polydimethylsiloxane, without fillers, exists as a liquid<sup>34</sup> and inherently lacks the necessary viscosity<sup>35</sup>, body, and mechanical strength required for clinical use as an impression material<sup>36</sup>. Therefore, incorporating standard reinforcing fillers like SiO2 and CaCO3 is essential in the control formulation to achieve these necessary functional characteristics and to establish a clinically relevant baseline against which the effects of the experimental fillers (DE and ZnO) can be accurately assessed. The specific compositions of the Control, Zn and DE pastes, including the varying volume fractions of the ZnO and DE additives, are detailed in Table 1.

Group	Sample Name	SiO2 (Vol%)	CaCO3 (Vol%)	ZnO (Vol%)	DE (Vol%)	PDMS-OH (Vol%)	TEOS (Vol%)	Total Volume (Vol%)
Control	Base Paste	54	6	0	0	39	1	100
	ZnO (0.5%)	53.5	6	0.5	0	39	1	100
	ZnO (1%)	53	6	1	0	39	1	100
Zn	ZnO (2%)	52	6	2	0	39	1	100
	ZnO (3%)	51	6	3	0	39	1	100
	ZnO (4%)	50	6	4	0	39	1	100
	DE (0.5%)	53.5	6	0	0.5	39	1	100
	DE (1%)	53	6	0	1	39	1	100
DE	DE (2%)	52	6	0	2	39	1	100
	DE (3%)	51	6	0	3	39	1	100
	DE (4%)	50	6	0	4	39	1	100

**Table 1**. Formulation of silicone pastes by volume (parts).

To achieve a homogeneous filler mixture with uniform dispersion of the microsized ZnO and DE powders (when present) within the other filler components, a planetary ball milling method was employed (Fig. 1a). This technique, owing to the high-impact collisions and shear forces generated between the balls and the materials, facilitates the uniform distribution of particles. For each paste formulation, the required filler powders (predetermined amounts of base fillers like silica and calcium carbonate, along with ZnO or DE powder if applicable) were weighed using a high-precision balance. This powder mixture was then placed into the zirconia jar of a planetary ball mill (AS2-600 model, Bonyan Faragir Sanat Mehrbin Co.). To increase the milling efficiency and prevent contamination, zirconia balls were utilized. The mixture was subsequently rotated for 2 h at a speed of 400 rpm. Following the milling process, the resulting powder was placed in an oven at 100 °C for 24 h to eliminate any potential moisture, as moisture can hydrolyze TEOS and potentially disrupt the silicone matrix. To prepare the silicone base paste, specific amounts of PDMS-OH and TEOS were added to the dried powder mixture. This step was carried out slowly via a mechanical stirrer (IKA\* RW 20 digital) to prevent air entrapment within the mixture. The stirring process was continued for two hours to ensure uniform dispersion of the filler powders within the polymer and crosslinker, resulting in the final base paste. This final paste was then mixed with the commercial activator (Speedex Universal Activator) according to the manufacturer's instructions to initiate the setting reaction and form the set impression material. The underlying chemical reaction mechanism for condensation curing is illustrated in Fig. 1b<sup>10,37</sup>.

#### Die preparation

For tensile analysis, dumbbell-shaped samples (Die C dimensions, ASTM D412, with a gauge length of 33 mm and width of 6 mm) were machined from stainless steel (Fig. 2a). The mold was subsequently attached to a polished, high-density polyethylene (HDPE) sheet. The sample fabrication involved loading the die with the prepared pastes, utilizing an HDPE sheet as the upper platen to ensure a flat surface. To assess the linear dimensional stability of the fabricated samples, a standardized ruled block (featuring critical ruled lines within a diameter of 29.97 mm, overall block height 31.0 mm) and a corresponding mold (a ring with a 30.00 mm internal diameter and 6.0 mm height) were constructed from polymethyl methacrylate (PMMA), ensuring a smooth and fine surface, in accordance with ANSI/ADA No. 19 and ISO 4823 standards (Fig. 2b). The pastes were loaded into the mold, and the ruled block was used to shape and compress the material.

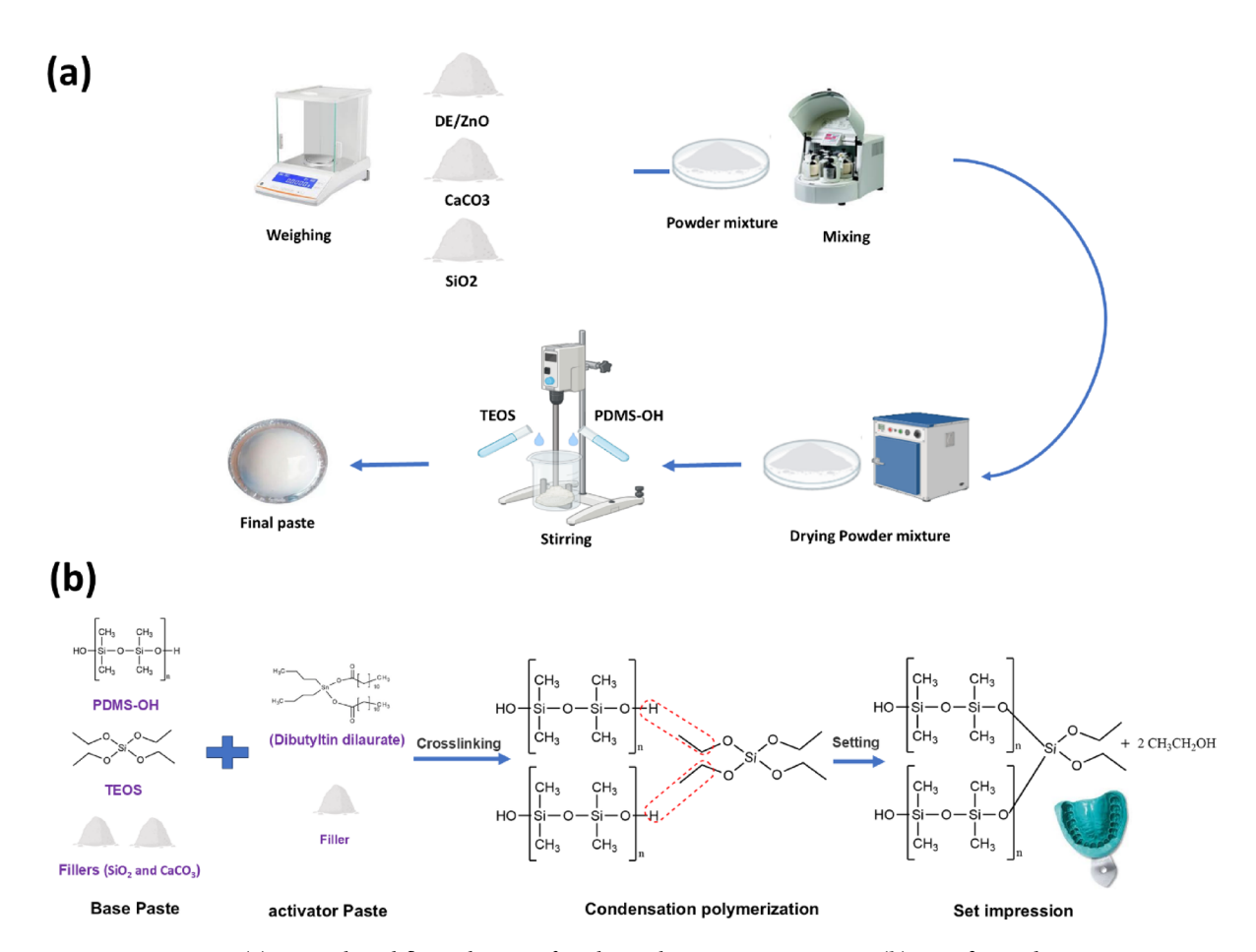


**Fig. 1.** (a) General workflow schematic for silicone base paste preparation. (b) Specific condensation polymerization mechanism showing the setting of silicone dental impression materials via crosslinking upon mixing base and activator components, releasing ethanol.

Fig. 2. (a) Schematic of a standard tensile test sample (ASTM D412). (b) Schematic of a ruled block for linear dimensional change measurements (ISO 4823).

#### Characterization

#### Mixing, setting, and working times

The mixing, working, and setting times were assessed for each sample (Control, Zn, DE) using freshly made paste according to ISO 4823, with five repetitions per test per group (n=5). The mixing time was determined at 25 °C by timing the process via a stopwatch (accurate to  $\pm$ 1 s over a 30 s period). This involved timing the period from the first contact of the base paste and the activator until a uniform mixture was achieved through hand kneading, indicated by a consistent color and texture. The working time was measured similarly, beginning at the start of mixing and concluding when the material became less fluid and showed elastic features. To determine the setting time, a timer was initiated upon the first contact of the components. After mixing, the paste was placed in a ring-shaped mold (like the one used for dimensional stability), with a sealed polyethylene sheet at the bottom. A Gillmore needle (initial-set type) with a tip diameter of 2.12 mm and a weight of 113.4 g was periodically dropped onto the paste surface every 15 s. The timer was stopped when the needle no longer left a mark, indicating the final setting time.

#### Scanning electron microscopy (SEM)

A TESCAN VEGA3 scanning electron microscope (SEM) equipped with an energy-dispersive X-ray spectroscopy (EDAX) detector was used to analyze the morphology and elemental composition of representative samples 24 h after setting. Elemental mapping was used to investigate the homogeneity of the samples.

#### Rheology

An Anton Paar Physica MCR 301 rheometer was employed to study the rheological properties of the prepared pastes (representative samples, approx. 5 g each) at 25 °C. This analysis, useing both rotational and oscillatory modes, provided data on the flow behavior and viscoelastic characteristics of the materials.

#### Dimensional stability

Dimensional stability was evaluated via impressions made with a standardized ruled block. Each impression was created by mixing the paste and activator at 25 °C, loading the resulting paste into the ring-shaped mold, and shaping it with the ruled block. Five replicate impressions (n=5) were made for each sample (Control, Zn, DE), adhering to ISO 4823 guidelines. Post-setting, the impressions were examined via an OLYMPUS DP72 optical microscope. The distances between parallel lines (a, b, c, d<sub>1</sub>, d<sub>2</sub> as defined in Fig. 2b) on the surface were measured at 30 min and 12 h after setting to assess short-term and long-term dimensional changes.

# Tensile properties

A SANTAM STM-20 universal testing machine (Iran) with a 2-ton capacity was used to evaluate the tensile properties of the materials, following the ASTM D412 standard. Five samples (n=5) were prepared for each sample (Control, Zn, DE). Testing was conducted 24 h after setting to assess the fully cured samples. Each sample underwent a 1-Newton preload at a crosshead speed of 5 mm/min, followed by an increase to 500 mm/min until rupture.

### Shore A hardness

Hardness was measured 24 h after setting to assess the fully cured samples using a Shore A durometer (Model SHD, SANTAM, Iran), in line with ASTM D-2240. Specimens were prepared with a thickness of at least 6 mm, as recommended by the standard. Measurements (n = 3 specimens, 5 measurements per specimen) were taken on a flat, parallel surface at 25 °C.

#### Wettability assessment

The surface wettability of the set impression material was assessed by measuring the static contact angle 24 h after setting. For each formulation (Control, Zn, DE), contact angle measurements were taken on five samples (n=5) via an MTN9.3-2021 optical tensiometer (from the Wetting and Interface Laboratory, Materials and Energy Research Center) equipped with IrCA94 software for analysis and reporting.

#### X-ray diffraction (XRD)

To analyze the crystalline structure, X-ray diffraction (XRD) was performed on representative powder and composite samples (24 h after setting) via a Seifert 3003 pts diffractometer (Germany) with a copper anode and Cu K $\alpha$  radiation ( $\lambda$  = 1.542 Å).

#### Antibacterial activity

The antibacterial activity of the samples was evaluated quantitatively against Gram-negative *Escherichia coli* (ATCC 25922, PTCC 1399) and Gram-positive *Streptococcus mutans* (IBRC-M 10682). The experimental procedure was based on the ISO 22196:2011 standard, with modifications. Test specimens (50 mm x 50 mm) were placed in sterile containers. The test was initiated 24 h after specimen setting to assess the stabilized material inherent properties, avoiding potential confounding effects from early-stage curing byproducts The test inoculum consisted of the bacterial strain suspended in 1/500 Nutrient Broth (NB); this medium was prepared by dissolving 3.0 g meat extract, 10.0 g peptone, and 5.0 g sodium chloride in 1000 ml water, then diluting this nutrient broth 500-fold with distilled water, and adjusting the pH to 6.8–7.2. A fresh bacterial culture was adjusted to a turbidity equivalent to 0.5 McFarland standard (1.5 ×  $10^8$  CFU/ml) and diluted in the 1/500 NB to approximately  $1.5 \times 10^6$  CFU/ml. 0.4 ml of this bacterial suspension (inoculum) was pipetted onto each test specimen surface, covered with a sterile 40 mm x 40 mm film, and pressed gently to create a thin film. The samples were incubated for (24±1) hours at (35±1)°C and a relative humidity of not less than 90%. Viable bacteria were recovered using 10 ml of SCDLP broth and counted after incubation on plate count agar (CFU-colony forming units). Each test was repeated three times (n=3). The Antibacterial activity (%) was calculated using Eq. (1):

Antibacterial activity (%) = 
$$\frac{(C-T)}{C} * 100$$
 (1)

where C is the average bacterial count from untreated Control samples and T is the average bacterial count from treated test samples after 24 h.

# Statistical analysis

All quantitative data requiring statistical comparison are presented as mean  $\pm$  standard deviation (SD), and statistical analyses were performed using Microsoft Excel 2021. Pairwise comparisons between each experimental sample (DE and Zn) and the Control sample were conducted for relevant quantitative properties using two-tailed independent samples t-tests assuming unequal variances. Differences were considered statistically significant at p < 0.05; where presented in figures, tables, and associated text, results significantly different from the control (p < 0.05) are noted as such, while non-significant differences (p > 0.05) are indicated as 'ns'.

# Results and discussion

To investigate the effects of ZnO and DE on the key properties of the condensation silicone impression dental materials, formulations containing 1 vol% ZnO (Zn sample) and 3 vol% DE (DE sample) were selected for detailed characterizationThis selection was based on a preliminary exploration of concentrations ranging from 0.5 vol% to 4 vol% for both additives, which revealed significant concentration-dependent changes in mixing behavior, workability, setting time, and dimensional stability. Compared to the control, 0.5 vol% ZnO had minimal effects on these properties. While 1 vol% ZnO showed potential benefits (discussed below), higher concentrations (2-4 vol%) led to a gradual increase in paste tackiness, negatively impacting mixing and workability. This became particularly problematic at 3 vol% and 4 vol%, where manual mixing became difficult or impossible. Thus, 1 vol% ZnO was chosen as the optimal concentration for detailed study, balancing potential benefits with acceptable workability. In contrast, DE had minimal effects on mixing behavior, workability, setting time, and dimensional stability at concentrations ranging from 0.5 vol% to 2 vol% compared with those of the control. However, at 4 vol%, DE significantly increased viscosity and altered viscoelastic behavior, severely hindering both mixing and workability. Despite these drawbacks at higher concentrations, 3 vol% DE was chosen as the lowest concentration exhibiting significant changes (e.g., in wettability) to investigate its potential to enhance other material properties, as discussed subsequently. On the basis of these findings, two series of experimental pastes were designed to further characterize the effects of 1 vol% ZnO and 3 vol% DE. In each series, ZnO or DE was substituted for SiO2 while maintaining a constant 60:40 volume ratio of fillers to liquid components (PDMS-OH and TEOS) to assess their individual effects on the paste properties. As shown in Table 1 (Materials and Methods section), increasing the volume fraction of either ZnO or DE ensures that the total filler volume remains constant at 60 vol%.

# Mixing, setting and working times

Figure 3 illustrates the setting time, working time, and mixing time of three distinct elastomeric impression material samples (Control, DE, and Zn), measured under standardized conditions per ISO 4823<sup>18</sup>. The analysis revealed significant differences in both setting and working times among the samples. Specifically, both the DE and Zn samples exhibited significantly longer setting times compared to the Control samples (p < 0.001). The Zn sample had the longest setting time, followed by the DE sample and then the control, with statistically significant differences observed among all three groups (p < 0.001 for all comparisons). Regarding working time, the Zn sample demonstrated a significantly longer working time compared to both the control and DE samples (p < 0.001). Conversely, the DE sample presented a significantly shorter working time than the control (p < 0.01).

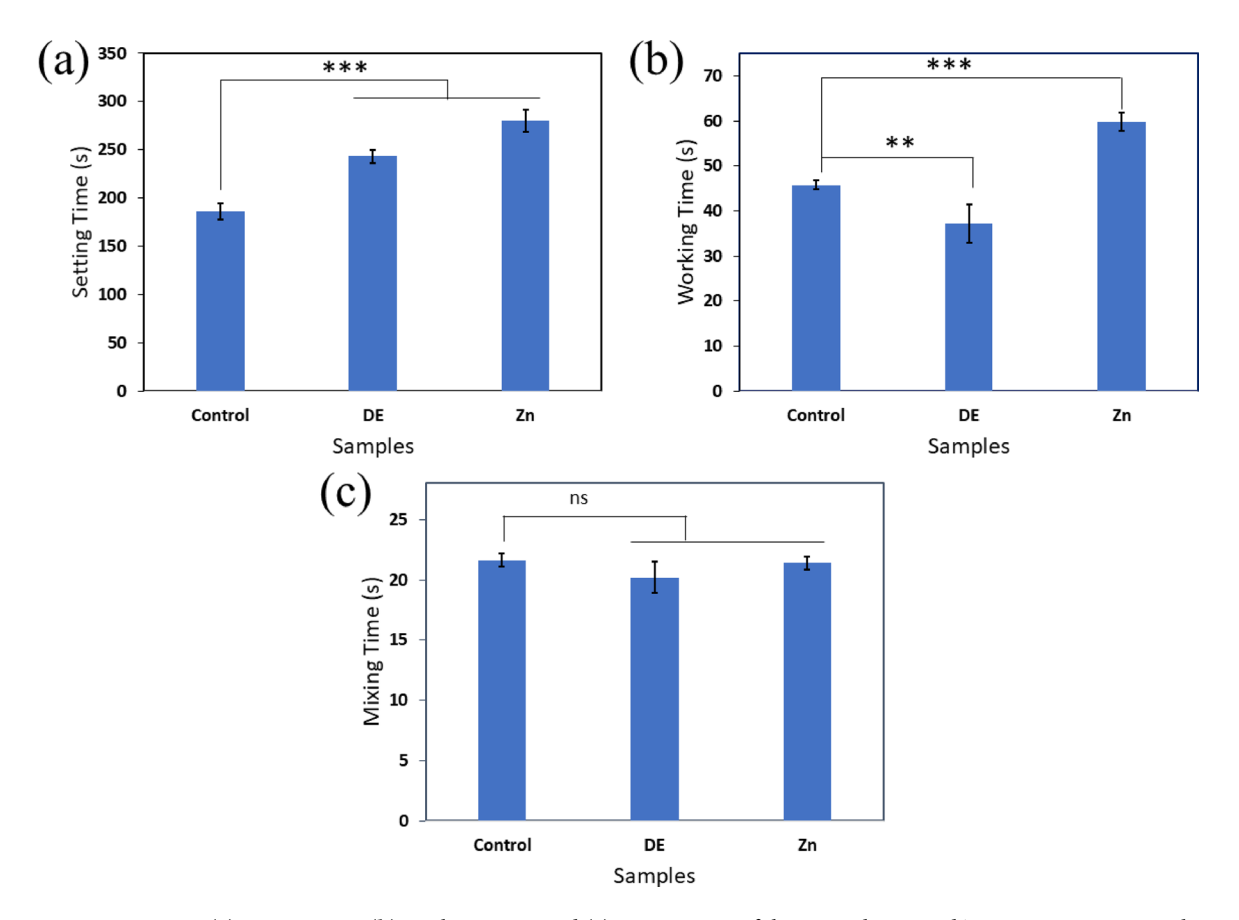


**Fig. 3.** (a) Setting time, (b) working time, and (c) mixing time of the control, DE, and Zn impression material samples. The error bars represent the standard deviation. Statistical significance: ns (not significant) p > 0.05, \*\* p < 0.01, \*\*\* p < 0.001.

In contrast to the setting and working times, no significant differences were found in the mixing times among the three samples (p > 0.05).

These findings highlight the distinct effects of the DE and Zn fillers, in comparison to the control, on the setting and working times of the impression pastes. The DE sample, in comparison to the control, exhibited a significantly shorter working time coupled with a longer setting time. This seemingly contradictory behavior can be attributed to the unique porous structure of DE. The DE structure facilitates significant surface adsorption and, notably, deep absorption of PDMS-OH oligomers<sup>38,39</sup>, which are crucial reactants in the condensation polymerization reaction. The absorption of PDMS-OH reduces the effective liquid-to-filler phase ratio, resulting in decreased workability of the paste and contributing to a shorter working time. This reduced workability may pose challenges for dentists, potentially hindering the accurate capture of details and increasing the likelihood of errors due to limited manipulation time before setting. Furthermore, the surface and deep absorption of PDMS-OH decreases the number of hydroxyl functional groups available for condensation polymerization, consequently prolonging the setting time<sup>40</sup>.

Conversely, the Zn sample exhibited both a significantly extended working time and setting time compared with those of the control. This can be attributed to the interaction between ZnO and the hydroxyl groups in PDMS-OH. ZnO is a highly polar (O = 3.5, Zn = 1.65 Pauling scale), amphoteric metal oxide. The oxygen atom in ZnO, which possesses lone pairs of electrons, can function as a Lewis base. It can form a coordinate covalent bond with the silicon atom in PDMS-OH, which has vacant d orbitals. In this bond, the oxygen atom of ZnO acts as the electron donor, whereas the silicon atom of PDMS-OH acts as the electron acceptor. The formation of coordinated covalent bonds and hydrogen bonds between ZnO and PDMS-OH reduces the availability of functional groups for the cross-linking reaction, thereby increasing the working and setting times<sup>41</sup>. In essence, by occupying the hydroxyl groups of PDMS-OH, ZnO limits their participation in cross-linking and setting reactions<sup>42</sup>. The extended working time offered by the Zn sample could be advantageous for dentists, particularly in complex cases, as it provides ample time to achieve a more precise impression.

# Rheology

The rheological properties of dental impression materials are critical to their clinical performance, dictating their ability to accurately capture intricate intraoral details while maintaining dimensional stability. These materials typically exhibit pseudoplastic (shear-thinning) behavior, characterized by a decrease in viscosity with

increasing shear rate<sup>43,44</sup>. This property facilitates easy flow and adaptation to oral tissues during impression, while ensuring sufficient viscosity at rest to preserve the impression shape<sup>45</sup>.

Figure 4 shows the rheological properties of the control, DE, and Zn impression pastes. As shown in Fig. 4a, all pastes exhibited shear-thinning behavior, with viscosity decreasing as shear rate increased. The Control paste had the highest initial viscosity (approximately 1000 Pa·s) at the start of the shear rate range, while the DE paste exhibited the lowest viscosity across all shear rates tested. Between approximately 1 s<sup>-1</sup> and 40 s<sup>-1</sup>, the Zn and DE pastes showed a nearly constant logarithmic decrease in viscosity, whereas the control paste exhibited a more gradual decrease.

This difference in viscosity can be attributed to the morphology of the fillers and their influence on interparticle interactions. The higher initial viscosity of the control paste at low shear rates may limit its ability to fully capture

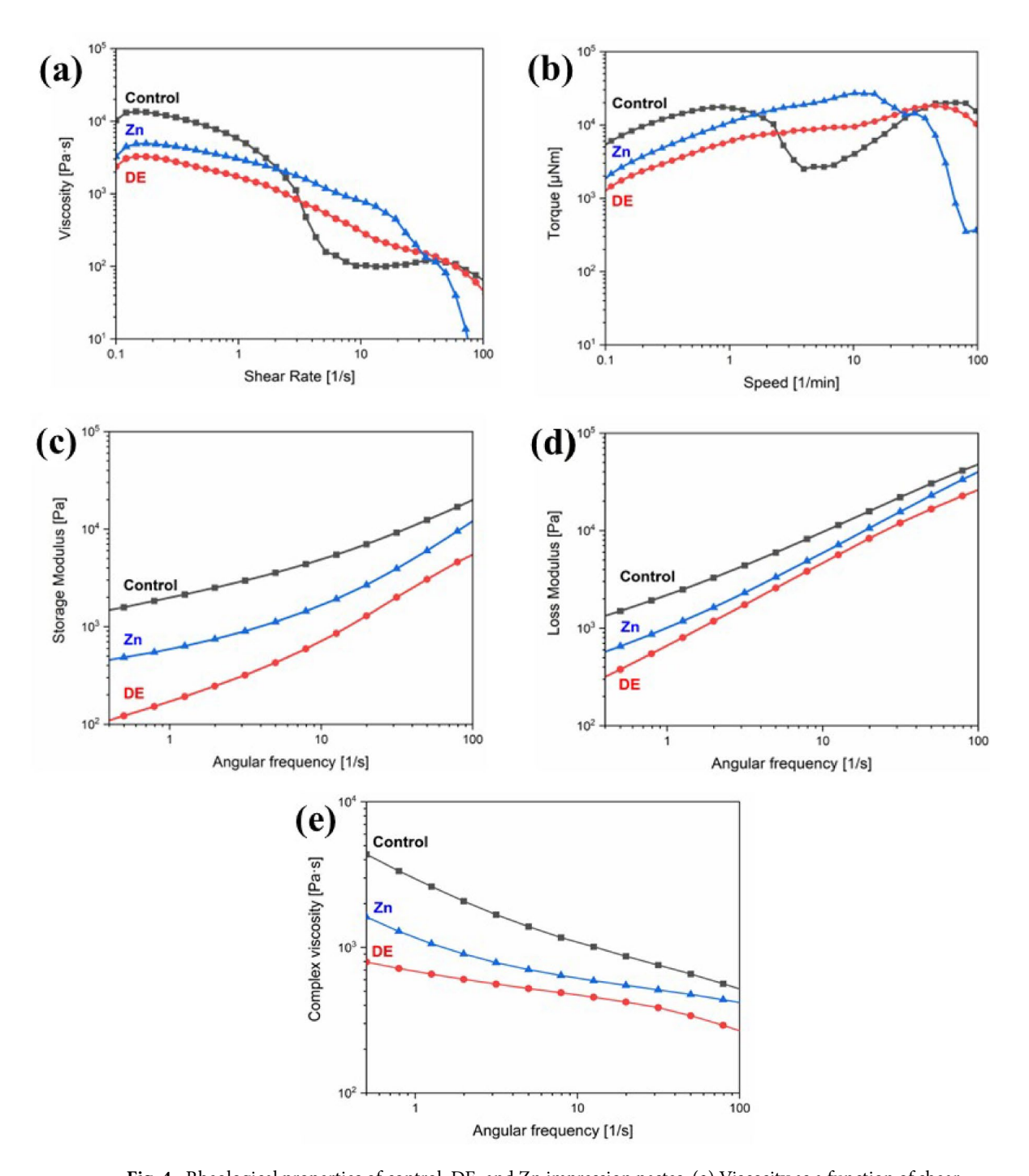


**Fig. 4.** Rheological properties of control, DE, and Zn impression pastes. (a) Viscosity as a function of shear rate. (b) Torque as a function of rotational speed. (c) Storage modulus (G') as a function of angular frequency  $(\omega)$ . (d) Loss modulus (G") as a function of angular frequency  $(\omega)$ . (e) Complex viscosity  $(\eta^*)$  as a function of angular frequency.

fine details. This is likely due to increased interparticle interactions arising from the morphology of the silica (sharp edges) and calcium carbonate (irregular shape) fillers, which can increase friction and interparticle bonding (Fig. 9). Conversely, the Zn and DE pastes exhibited lower viscosities at low shear rates, indicating improved flow characteristics. This suggests that these materials may be better able to flow into and capture fine details within the oral cavity. SEM analysis (Fig. 9) revealed that the DE paste, with its diverse range of particle shapes (irregular shards, spherical particles, and hollow tube-like structures), disrupts efficient packing and reduces interparticle contact<sup>19</sup>. Similarly, the needle-like structure of the ZnO particles in the Zn paste may also interfere with efficient packing, leading to lower viscosity. Furthermore, the alignment of these needle-like ZnO particles under shear could contribute to the lower viscosity by facilitating slippage and reducing resistance to flow<sup>46,47</sup>. The torque-speed profiles shown in Fig. 4b mirror the observed viscosity trends.

Figure 4e illustrates the relationship between the complex viscosity ( $\eta^*$ ) and angular frequency. The Control paste presented the highest complex viscosity, whereas the DE paste presented the lowest, a trend consistent across the entire range of angular frequencies tested. The Zn paste maintains an intermediate  $\eta^*$ .

Analysis of the storage modulus (G) (Fig. 4c) revealed frequency-dependent behavior. Figure 4c shows the storage modulus (G) of the pastes, where at  $\omega = 1$  s<sup>-1</sup>, the control paste exhibited the highest storage modulus (G), followed by the Zn paste and then the DE paste. In fact, G increased with increasing  $\omega$  for all pastes. The Control paste also presented the highest G, followed by the Zn paste and then the DE paste, as shown in Fig. 4d. Both G and G increased with increasing  $\omega$  for all pastes. At an angular frequency ( $\omega$ ) of 1 s<sup>-1</sup>, the control paste exhibited the highest G, followed by the Zn paste and then the DE paste. G increased with increasing  $\omega$  for all pastes. The Control paste exhibited the highest G across all frequencies, indicating a greater degree of elastic behavior and a stronger network structure within the paste. This is presumably due to greater hydrogen bonding and van der Waals forces between the polymer oligomers and increased particle-particle interactions<sup>42</sup>. Conversely, the lower G of the DE paste suggests a less developed or more easily disrupted internal network, which may potentially lead to greater susceptibility to permanent deformation<sup>24</sup>. The Zn paste, containing needle-like ZnO particles, presented intermediate G values, indicating a balance between elastic and viscous responses.

The loss modulus (G") (Fig. 4d) followed a similar trend (Control>Zn>DE) and also increased with increasing  $\omega$  for all pastes. The control paste exhibited the highest G", reflecting greater energy dissipation during deformation, which is consistent with its more robust network structure. The significantly lower G" of the DE paste suggests reduced interparticle friction and lower energy dissipation<sup>23</sup>. The Zn paste, despite its intermediate G", displayed a lower complex viscosity ( $\eta^*$ ) than the control, suggesting enhanced flowability<sup>44</sup>. This enhanced flowability of the Zn paste could be attributed to the alignment of the needle-like ZnO particles under shear, potentially creating a lubricating effect that facilitates flow while maintaining a degree of structural integrity<sup>48</sup>.

#### Dimensional stability

The dimensional stability of Control, DE, and Zn samples was evaluated by measuring linear dimensional changes at 30 min and 12 h after setting (Figs. 5 and 6). Across all measured dimensions (a-b, b-c, a-c, and d1-d2) and at both time points, the Zn samples exhibited significantly less shrinkage compared to the control (p < 0.05, p < 0.01, or p < 0.001), highlighting their positive impact on dimensional stability. Conversely, the DE sample did not improve dimensional stability. At 30 min, the b-c and a-c measurements for the DE sample showed significantly greater shrinkage than the Control (p < 0.05 and p < 0.01, respectively), with a similar level of significance observed at 12 h (p < 0.01). While other measurements for the DE samples were not significantly different from the control, the overall data indicates that the DE filler did not offer any improvement and may have exacerbated shrinkage in certain dimensions.

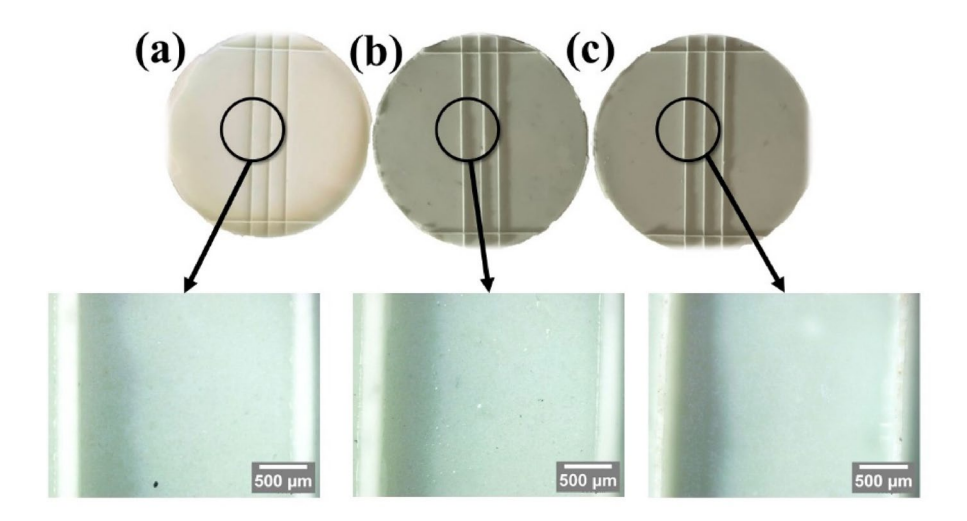
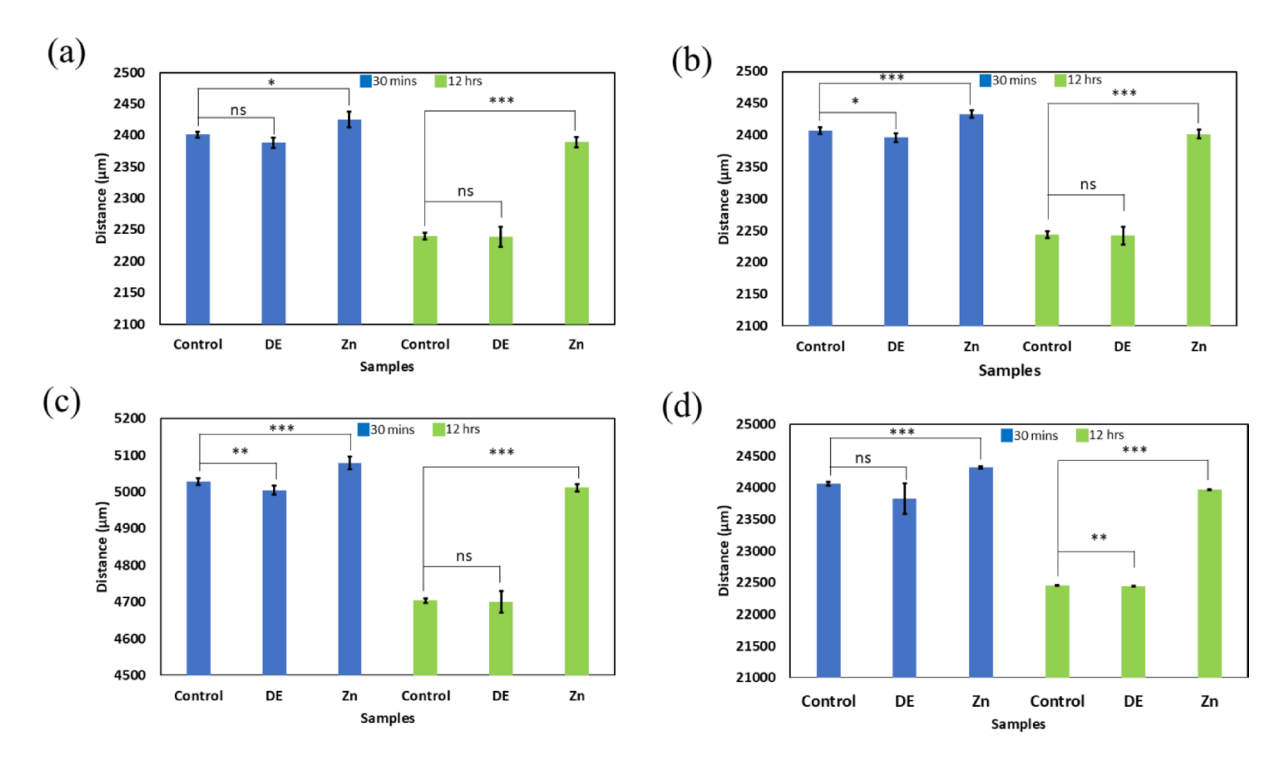


Fig. 5. Dimensional stability of Zn, DE, and control samples. Top row: Samples 30 min postfabrication. Bottom row: Optical microscope images of the lines used to measure dimensional changes (scale bars =  $500 \mu m$ ). Measured distances: Zn =  $2436 \mu m$ , DE =  $2391 \mu m$ , control =  $2401 \mu m$ .



**Fig. 6.** Effect of filler type and time on the dimensional stability of samples. Charts represent the mean distance ( $\mu$ m) between lines for different filler types (Control, DE, and Zn) at 30 min (blue bars) and 12 h (green bars) for four different measurement sets: (**a**) a-b, (**b**) b-c, (**c**) a-c, and (**d**) d1-d2. The error bars represent the standard deviations. Statistical significance compared with the control at each time point is indicated: ns (not significant) p > 0.05, \*p < 0.05, \*p < 0.05, \*p < 0.01, \*\*\* p < 0.001.

Condensation silicone impression materials shrink due to the release of volatile byproducts during the condensation reaction  $^{49}$ . Minimizing this shrinkage and achieving isotropic shrinkage are critical for accurate dental impressions  $^{50}$ . Evaluating dimensional changes at both 30 min and 12 h, as performed here, allows characterization of the shrinkage kinetics inherent to condensation silicones. This timeframe captures both rapid initial contraction and more prolonged stabilization, providing clinically relevant data for determining optimal cast pouring times. The consistent reduction in shrinkage observed with the Zn samples aligns with ZnO's established reinforcing properties  $^{29}$ . SEM analysis (Fig. 11) revealed a homogeneous distribution of needle-like ZnO particles, approximately 1  $\mu$ m in size, within the silicone matrix of the Zn sample. This uniform dispersion likely contributes to the observed reduction in shrinkage, as the ZnO particles may effectively occupy potential voids within the silicone matrix, restricting polymer chain movement during polymerization and consequently mitigating shrinkage  $^{51}$ .

# Tensile properties

Figure 7; Table 2 present the stress-strain curves and corresponding tensile test data for the control, Zn, and DE samples, highlighting key differences in their mechanical behavior. Testing at 24 h post-setting ensured evaluation of the materials' stable mechanical response after substantial completion of the condensation curing reaction. The Control and DE samples exhibit similar initial slopes in the elastic region, confirmed by their comparable elastic moduli  $(4.27 \pm 1.02 \text{ MPa}$  and  $4.31 \pm 1.12 \text{ MPa}$ , respectively), indicating similar stiffness. This similarity in elastic moduli, however, appears to contradict the rheological analysis (Fig. 4a), where the Control paste exhibited a significantly higher storage modulus (G') than the DE paste across all frequencies (Fig. 4c). This apparent conflict between tensile stiffness (measured on the set solid) and rheological stiffness (measured on the paste) occurs because the two methods evaluated the material in fundamentally different states: uncured paste versus cured solid<sup>52</sup>.

In contrast to the Control and DE samples, the Zn sample displays a visibly lower initial slope and a correspondingly lower elastic modulus ( $2.35\pm1.14$  MPa), suggesting greater flexibility. This lower modulus, while potentially advantageous for adapting to complex dental structures (consistent with its lower viscosity and enhanced flow properties), surprisingly did not compromise dimensional stability (as shown previously). This can likely be attributed to the homogeneous distribution of needle-like ZnO particles (observed via SEM), which effectively reinforce the silicone matrix and restrict polymer chain movement during polymerization, as previously discussed 1. The Zn sample also exhibited the highest elongation at break (64.16  $\pm$ 1.21%), indicating good ductility but potentially lower ultimate tensile strength. While a lower ultimate tensile strength might raise concerns about the material's ability to withstand stress without permanent deformation 4, the Zn sample demonstrated the highest dimensional stability, suggesting its suitability for applications where dimensional accuracy is critical. The DE sample's stress-strain curve reveals a pronounced yield point, followed by plastic

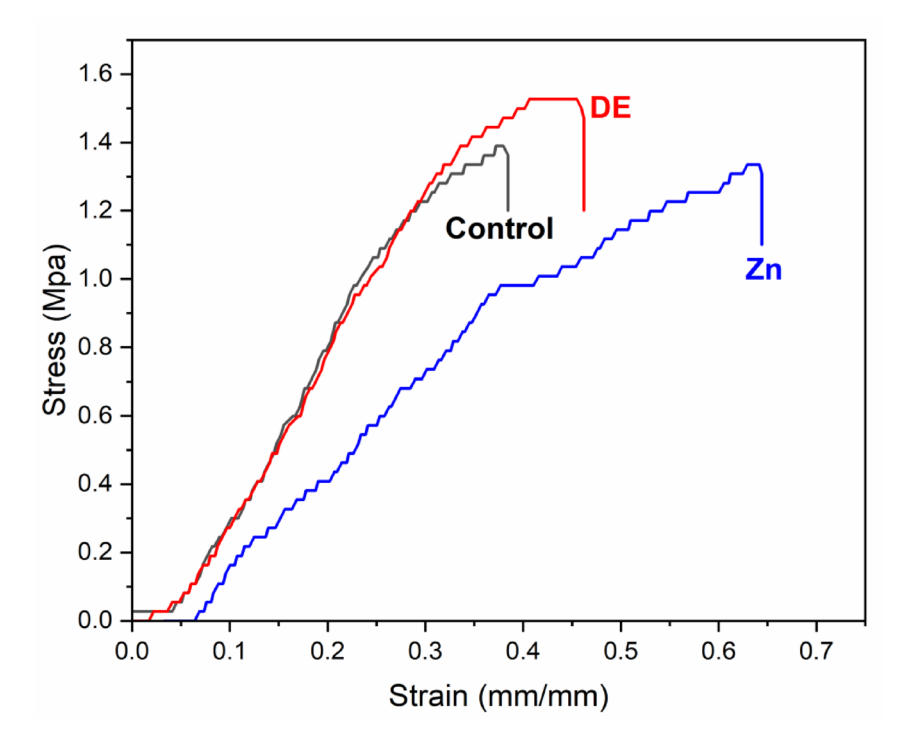


Fig. 7. Stress-strain curves of three samples: control, Zn and DE.

Sample	Force (N)	Extension (mm)	Elongation (%)	Elastic Modulus (MPa)
Control	25.00 +/- 1.21	12.52 +/- 1.09	37.94 +/- 1.26	4.27 +/- 1.02
DE	27.46 +/- 0.98	15.01 +/- 0.99	45.48 +/- 1.07	4.31 +/- 1.12
Zn	24.03 +/- 1.09	21.17 +/- 0.93	64.16 +/- 1.21	2.35 +/- 1.14

**Table 2**. Tensile test results for the control, DE, and Zn samples. The values are presented as the means ± standard deviations.

Samples	Mean	Std. Deviation	
Control	62	1.41	
DE	56***	1	
Zn	55***	1	

**Table 3**. Shore A hardness of control, DE, and Zn samples (Mean  $\pm$  Std. Deviation)\*. \*\*\* p < 0.001 compared to Control.

deformation before failure. This distinct yield point and greater ductility compared to the control likely contribute to its ability to withstand deformation during removal without tearing. This behavior may be attributed to the specific surface area, hollow structure, and low density of the DE particles, which can promote interparticle bonding and energy dissipation<sup>52,55,56</sup>.

#### Shore A hardness test

Shore A hardness, a measure of a material resistance to indentation, is a crucial property in dental impression materials, influencing their ability to capture fine details, withstand stress, and support the casting process  $^{57,58}$ . Hardness measurements were performed according to ASTM D-2240 (Table 3). As with tensile properties, the 24-hour post-setting measurement provides hardness values representative of the fully cured silicone network, allowing for valid comparisons between the filler effects. The results revealed that the Control exhibited the highest Shore A hardness  $(62\pm1.41)$ , while both the DE sample  $(56\pm1.00)$  and the Zn sample  $(55\pm1.00)$  had significantly lower (p<0.001) values compared to the Control. The low standard deviations for all three materials indicate consistent hardness within each sample set.

While the Control higher hardness suggests superior resistance to deformation, this must be considered alongside other mechanical properties. Interestingly, despite their lower hardness, the Zn samples demonstrated

Samples	Mean[°]	Std. Deviation [°]
Control	108.32	2.37
DE	102.37	1.45
Zn	106.24	1.39

**Table 4**. Contact angle measurements of water droplets on control, DE, and Zn samples (Mean ± Std. Deviation).

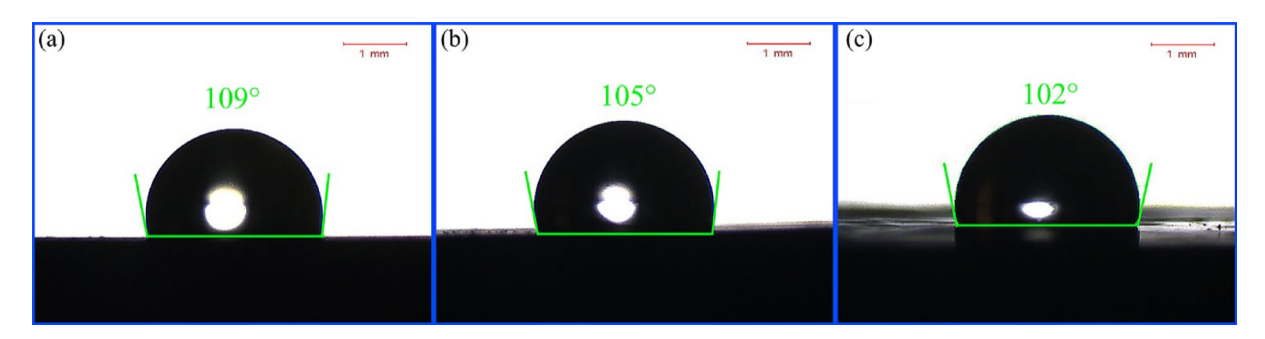


Fig. 8. Wettability of the (a) control, (b) Zn, and (c) DE samples.

the highest dimensional stability. This suggests that factors beyond simple hardness, such as inherent elasticity and recovery from deformation, are crucial for dimensional accuracy. This observation aligns with the tensile test results, where Zn exhibited the highest ductility (elongation at break), indicating a greater capacity for elastic deformation than the DE and Control samples. The significantly lower hardness of the DE and Zn samples suggests greater flexibility, potentially advantageous for patient comfort and improved detail capture, particularly in undercut areas, as suggested by their lower viscosity and enhanced flow properties. However, their lower hardness necessitates careful handling to avoid distortion during impression removal<sup>59</sup>. Finally, the observed differences in hardness may be related to variations in the elemental composition of the samples, particularly the concentration of calcium (higher in Control, see EDAX results, Fig. 10)<sup>57,60</sup>.

# Wettability

The wettability of dental impression materials is crucial for accurately capturing the fine details of oral tissues and subsequently for the interaction with gypsum slurry when pouring the cast. Measurements were performed 24 h post-setting, reflecting the surface state after the majority of volatile byproduct (ethanol) evaporation, which could otherwise alter surface tension and contact angle measurements. This timing is relevant as it corresponds to a period when casts are typically poured onto a fully set impression. Results (Table 4; Fig. 8) demonstrate the impact of incorporating DE and ZnO on this property. The Control sample exhibited the highest contact angle  $(108.32^{\circ} \pm 2.37^{\circ})$ , indicating the low est wettability and potentially limiting its adaptation to moist oral tissues. This is consistent with its higher viscosity at low shear rates, which could further hinder flow and wetting of intricate surfaces.

In contrast, incorporating DE significantly enhanced wettability, resulting in the lowest contact angle ( $102.37^{\circ} \pm 1.45^{\circ}$ ). This improvement likely stems from the porous structure of DE, which may facilitate the release of low-molecular-weight components (e.g., unreacted oligomers) onto the material's surface in contact with water droplets, effectively increasing hydrophilicity. The addition of ZnO also moderately improved wettability ( $106.24^{\circ} \pm 1.39^{\circ}$ ), likely due to the increased surface area provided by the microsized filler, leading to greater adsorption. Furthermore, the wurtzite structure of ZnO, confirmed by XRD analysis, may contribute to increased wettability by promoting interactions with water molecules. While the improvement with ZnO was less pronounced than with DE, it still represents an enhancement over the control and may contribute to the enhanced flow and detail capture observed in the Zn samples. Overall, both DE and ZnO improved the wettability of the impression material compared to the control, with DE demonstrating a more substantial effect.

#### **SEM and EDAX analysis**

Scanning electron microscopy (SEM) analysis revealed the distinct morphologies of the different powders.  $CaCO_3$  consisted of particles with irregular shapes and a rough surface texture (Fig. 9a), while  $SiO_2$  quartz had angular particles with sharp edges and a smoother surface (Fig. 9b). ZnO exhibited a predominantly needle-like morphology (Fig. 9c), and the DE powder had a heterogeneous microstructure with a wide variety of diatom frustule morphologies, including elongated, cylindrical forms, disc-like forms, and fragmented frustules (Fig. 9d).

EDAX analysis (Fig. 10) confirmed the presence of key elements in each sample. The Control primarily comprised carbon, oxygen, silicon, and calcium. The DE sample additionally showed peaks for aluminum and iron, confirming the incorporation of diatomaceous earth. The Zn sample exhibited a prominent zinc peak. The

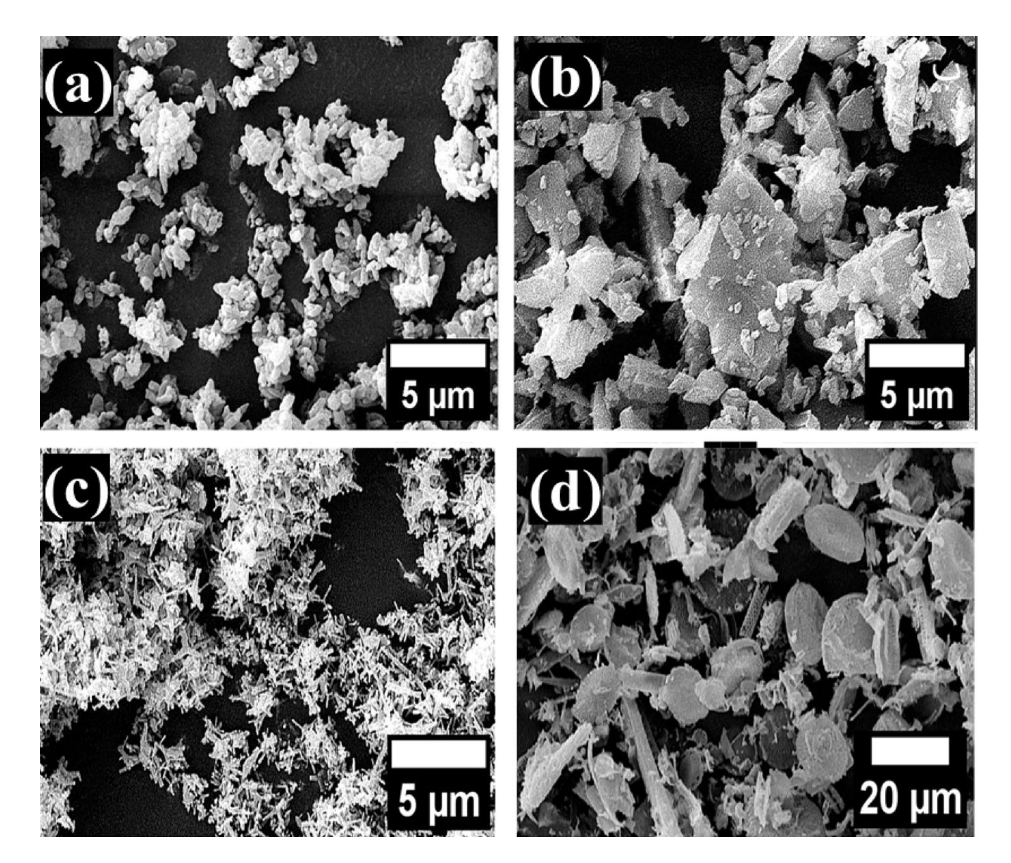


Fig. 9. SEM images of (a) CaCO<sub>3</sub>, (b) SiO<sub>2</sub>, quartz, (c) ZnO powder and (d) DE powder.

gold (Au) peak, originating from the sputter coating applied to enhance sample conductivity, was disregarded in the analysis.

The elemental maps (Fig. 11) provided a visual representation of the elemental distribution within the samples. These maps clearly showed the uniform distribution of carbon and silicon, the base elements of the condensation silicone impression matrix. Calcium was dispersed relatively evenly in the Control sample. The DE sample showed a distinct localization of aluminum within the larger surface aggregates (corresponding to DE particles), and the Zn sample exhibited a homogeneous dispersion of zinc.

The observed microstructures provide insights into the material properties. The heterogeneous and porous microstructure of the DE powder is expected to disrupt efficient packing and reduce interparticle contact within the composite material, potentially leading to a reduction in density and an increase in porosity<sup>19</sup>. The needle-like morphology of the ZnO particles observed via SEM suggests a potential reinforcing effect within the matrix, potentially influencing properties like elongation percentage and tear strength<sup>53,62</sup>. The higher calcium concentration in the Control sample (EDAX results) provides a possible explanation for its higher Shore A hardness value (Table 3). This finding highlights the interconnectedness of material composition, microstructure, and mechanical properties<sup>63,64</sup>. Finally, the uniform distribution of elements observed in the elemental maps (Fig. 11) confirms the successful incorporation of ZnO and DE powder into the silicone matrix while maintaining the stability of the base polymer material.

#### XRD analysis

X-ray diffraction (XRD) analysis was performed on the DE and ZnO powders, as well as on the set Zn, DE, and Control samples. As shown in Fig. 12, the control sample displayed diffraction peaks corresponding to both quartz ( $\alpha$ -quartz) and calcite. The ZnO powder exhibited a series of sharp, well-defined peaks indicative of a highly crystalline structure, aligning with the hexagonal wurtzite structure of ZnO. The Zn sample retained characteristic ZnO peaks but with a reduced intensity compared to the pure powder, as expected due to its lower concentration in the composite. The XRD patterns of both DE powder and the DE sample revealed the presence of cristobalite, a crystalline form of silica.

Each sample displayed distinct crystalline phases and structural characteristics, highlighting the effects of the ZnO and DE powders as additives. While the crystalline nature confirmed the filler phases, the enhanced dimensional stability observed for the Zn sample is more directly attributed to the reinforcing effect of ZnO particles. This effect, related to ZnO's high modulus of elasticity, strong particle-matrix interaction, and ability to restrict polymer chain movement, contributes to its ability to limit shrinkage and maintain dimensional accuracy<sup>31</sup>. The relative intensities of the peaks in the DE sample were slightly lower than those in the DE powder pattern, which is expected because of the lower concentration of diatomaceous earth in the composite matrix.

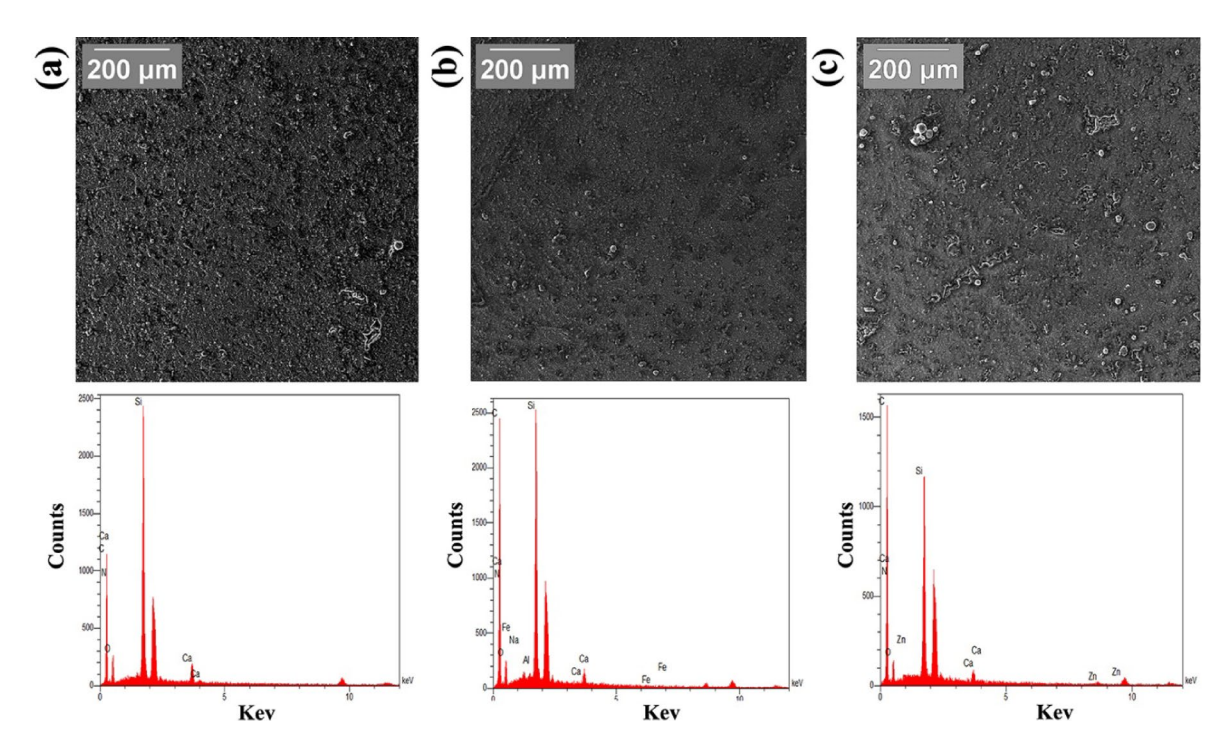
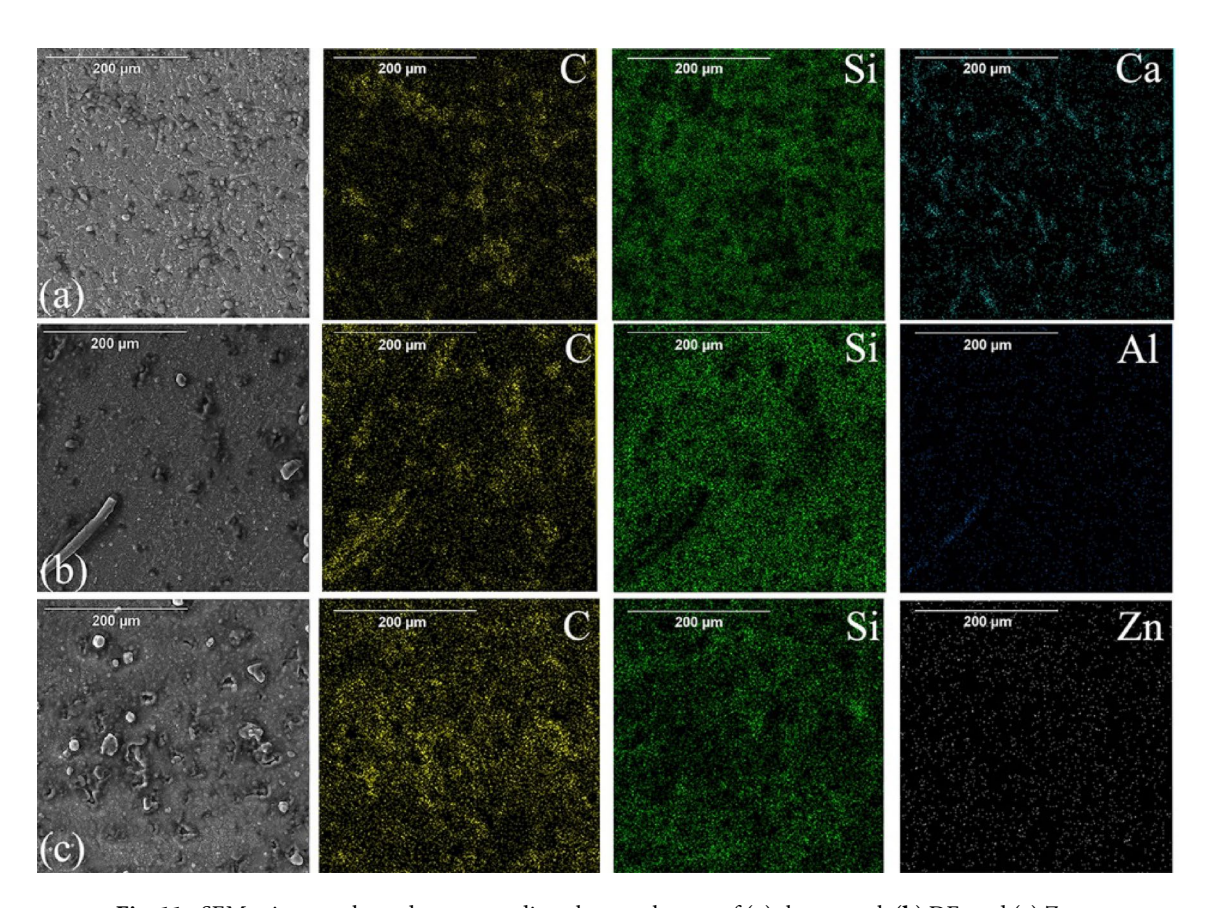


Fig. 10. SEM images and corresponding EDAX spectra of the (a) control, (b) DE, and (c) Zn samples.



 $Fig.\ 11.\ \ \text{SEM micrographs and corresponding elemental maps of (a) the control, (b) DE, and (c) Zn.}$ 

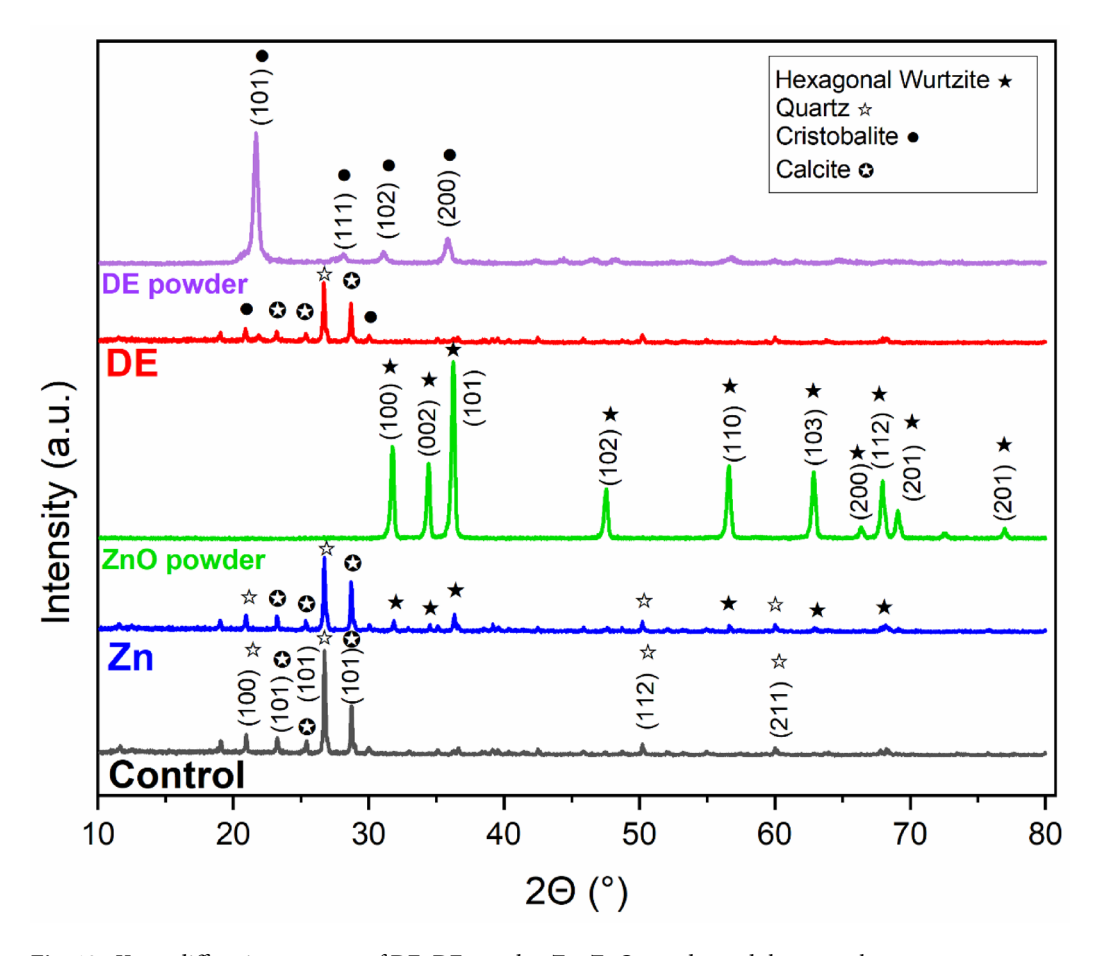


Fig. 12. X-ray diffraction patterns of DE, DE powder, Zn, ZnO powder and the control.

Sample	E. coli Count (Mean ± Std. Deviation, CFU/ml)	E. coli Antibacterial Activity (Mean ± Std. Deviation, %)	S. mutans Count (Mean±Std. Deviation, CFU/ml)	S. mutans Antibacterial Activity (Mean ± Std. Deviation, %)
Zn	$(3.0 \pm 0.05) \times 10^5$	80±2	$(7.8 \pm 0.05) \times 10^5$	48±3
DE	$(1.4 \pm 0.03) \times 10^6$	5±1	$(1.4 \pm 0.04) \times 10^6$	5±2
Control	$(1.4 \pm 0.04) \times 10^6$	6±1	$(1.4 \pm 0.04) \times 10^6$	6±1
Blank	$(1.5 \pm 0.00) \times 10^6$	*	$(1.5 \pm 0.00) \times 10^6$	*

**Table 5**. Antibacterial activity (%) and bacterial counts (CFU/ml) for Zn and DE samples against E. coli and S. mutans (24 h incubation). Data are mean ± standard deviation.

# **Antibacterial activity**

The antibacterial activity of the DE, Zn and control samples was evaluated against *E. coli* and *S. mutans*, two common oral bacteria. Testing was initiated after 24 h to ensure that the measured antimicrobial effects were attributable to the stabilized material and incorporated fillers (ZnO), rather than the transient bactericidal effect of the evaporating ethanol byproduct. As shown in Table 5; Fig. 13, the Zn sample exhibited potent antibacterial effects, with an antibacterial activity against E. coli of  $(80\pm2)\%$  and against S. mutans of  $(48\pm3)\%$  compared to the control  $(6\pm1)\%$ . In contrast, the DE sample showed minimal antibacterial effects, with  $(5\pm1)\%$  activity against E. coli and  $(5\pm2)\%$  activity against S. mutans, values similar to the activity observed in the control sample  $((6\pm1)\%$  for E. coli and  $(6\pm1)\%$  for S. mutans).

This superior antibacterial efficacy of the Zn samples aligns with the well-established antimicrobial properties of zinc ions<sup>65</sup>. Zn<sup>2+</sup> ions exert bactericidal effects by disrupting bacterial cell membrane integrity, interfering with enzyme activity, and inducing oxidative stress<sup>27,66,67</sup>. Conversely, the negligible antibacterial activity of the DE samples is consistent with the inherent lack of antimicrobial properties associated with diatomaceous earth<sup>22</sup>.

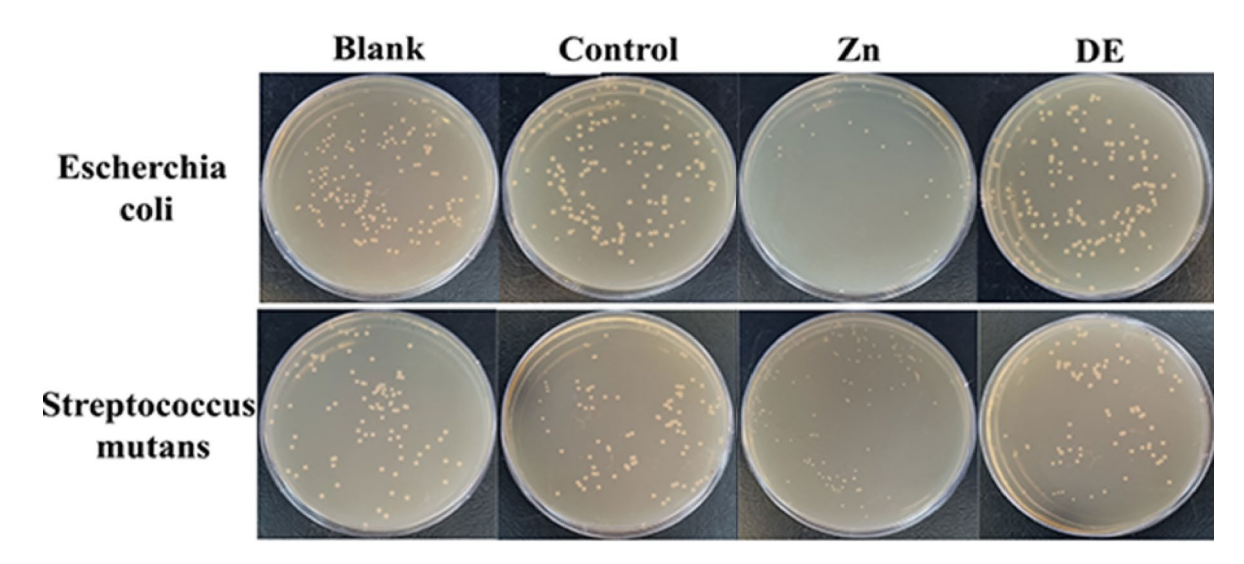


**Fig. 13.** Antibacterial activity of impression materials incorporating ZnO and DE against Escherichia coli and Streptococcus mutans. Agar plates showing bacterial growth after 24 h of incubation.

# Conclusion

This study investigated the effects of incorporating diatomaceous earth (DE) and zinc oxide (ZnO) fillers into a condensation silicone impression material compared to a control group containing only silica and calcium carbonate fillers. Both fillers significantly altered the material's properties. The Zn samples enhanced the dimensional stability, extended the working and setting times, improved the flowability, and moderately enhanced the wettability. The lower elastic modulus and increased flexibility of the Zn samples could also improve patient comfort and ease of removal. The DE samples significantly improved wettability and flowability while decreasing Shore A hardness, potentially increasing patient comfort. However, DE samples did not significantly affect dimensional stability relative to the control and resulted in a shorter working time. The DE samples also exhibited greater ductility. Importantly, Zn samples imparted significant antibacterial activity against *E. coli and S. mutans*, whereas the DE samples had no effect in this regard. In conclusion, incorporating DE and ZnO influenced the material properties differently, highlighting distinct potential applications: ZnO offers significant improvements in functional properties crucial for clinical accuracy and hygiene (dimensional stability, working time, antibacterial activity), whereas DE primarily modifies surface and flow characteristics, albeit with compromises in stability and handling time. This demonstrates the potential for targeted material design through careful filler selection based on desired outcomes.

# Data availability

Data will be made available on request. Requests for data access should be directed to the corresponding author, Saeed Hesaraki, at S-hesaraki@merc.ac.ir.

Received: 13 March 2025; Accepted: 7 July 2025

Published online: 13 July 2025

#### References

- Bennani, V., Inglesias, G. & Samson, J. Accuracy of intraoral digital impressions for fixed prosthodontics: A systematic review. J. Prosthet. Dent. 125 (1), 34–42 (2021).
- 2. Alshehri, F. A., AlHarbi, F. A. & AlQahtani, A. S. and others, The effect of impression techniques on the accuracy of complete-arch digital impressions: A systematic review, *J Prosthodont Res*, vol. 65, no. 3, pp. 299–307, (2021).
- 3. Abduo, J. & Lyons, K. Clinical considerations for impression materials. *Inside Dentistry*. 8 (2), 74–83 (2012).
- 4. Mangani, F. M., Hauschild, U. & Hübscher, W. Elastomeric impression materials: A review of the current state of the Art. *Dent. Mater.* **33** (6), 691–703 (2017).
- 5. Haoran, M. A. Digital versus conventional impressions for fixed prosthodontics: A review. *Jdoh* 9 (1), 1–11. https://doi.org/10.173 03/jdoh.2022.9.104 (2022).
- 6. Hämmerle, C. H. F. et al. The effect of tray selection on the accuracy of implant impressions: A systematic review. *Int. J. Oral Maxillofac. Implants* 35, 2 (2020).
- Graiff, L., Schaer, R. & Strub, J. R. Accuracy assessment of implant impressions: A systematic review of in vitro studies. Clin. Oral Implants Res. 33 (10), 1081–1092 (2022).
- 8. Shen, C., Rawls, H. R. & Esquivel-Upshaw, J. F. Phillips' Science of Dental Materials E-Book: Phillips' Science of Dental Materials E-Book (Elsevier Saunders, 2021).
- 9. Hammoodi, O. A., Rejab, L. T. & Alwattar, W. T. Evaluation The Accuracy Of Modified Closed Tray Impression Technique For Multiple Angled Implants Using Condensation-Silicone Impression Material, *University of Mosul*, vol. 13, no. 3, pp. 413–422, Jun. (2020). https://doi.org/10.33899/RDEN.2020.165367
- 10. Jurásková, A., Dam-Johansen, K., Olsen, S. M. & Skov, A. L. Factors influencing mechanical long-term stability of condensation curing silicone elastomers. J. Polym. Res. 27 (11), 1–14. https://doi.org/10.1007/S10965-020-02272-5/METRICS (Nov. 2020).
- 11. Christensen, G. J. Impression materials: state of the Art. Dent. Clin. North. Am. 54 (1), 1-13 (2010).

- 12. Walker, M. P., Burtschi, S. & Tsakona, A. Evaluation of the detail reproduction and dimensional accuracy of ten elastomeric impression materials. *J. Dent.* 38 (5), 387–393 (2010).
- 13. Sinobad, T. et al. Feb., The effect of disinfectants on dimensional stability of addition and condensation silicone impressions, Vojnosanit Pregl, vol. 71, no. 3, pp. 251–258, (2014). https://doi.org/10.2298/2227
- 14. Kim, K. C., Park, C. J. & Lee, Y. K. The effect of filler particle size on the physical properties of experimental dental composites. *Dent. Mater. J.* 26 (4), 578–585 (2007).
- 15. Grundke, K., Michel, S., Knispel, G. & Grundler, A. Wettability of silicone and polyether impression materials: Characterization by surface tension and contact angle measurements, *Colloids Surf A Physicochem Eng Asp*, vol. 317, no. 1–3, pp. 598–609, Mar. (2008). https://doi.org/10.1016/j.colsurfa.2007.11.046
- Mohd, N. R., Omar, R. A. & Etajuri, E. A. Dimensional Stability of Elastomeric Impression Material After Disinfection Via Immersion and Microwave Irradiation, Open Dent J, vol. 15, no. 1, pp. 658–663, Jan. (2021). https://doi.org/10.2174/1874210602115010658
- 17. Abhijeet, K., Jei, J. B., Murugesan, K. & Muthukumar, B. Evaluation of setting time, tear strength, dimensional stability and antimicrobial property of silver and titanium nanoparticles incorporated elastomeric impression material, *J Oral Biol Craniofac Res*, vol. 12, no. 5, pp. 547–551, Sep. (2022). https://doi.org/10.1016/j.jobcr.2022.07.002
- 18. Reddy, M. S. et al. Evaluation of antimicrobial activity and physical properties of vinyl siloxane ether impression material modified with zinc oxide and Chitosan nanoparticles: an In-vitro study. *J. Clin. Diagn. Res.* 18, 7 (2024).
- 19. Reka, A. A. et al. Diatomaceous earth: characterization, thermal modification, and application. *Open. Chem.* 19 (1), 451–461 (2021).
- 20. Guiraldo, R. D. et al. Characterization of morphology and composition of inorganic fillers in dental alginates, *Biomed Res Int*, vol. no. 1, p. 178064, 2014, (2014). https://doi.org/10.1155/2014/178064
- 21. Maher, S., Kumeria, T., Aw, M. S. & Losic, D. Diatom silica for biomedical applications: recent progress and advances. Adv. Healthc. Mater. 7 (19), 1800552 (2018).
- Chung, C. C. & Hwang, J. J. Porous diatomaceous Earth/Nano-Zinc oxide composites: Preparation and antimicrobial applications. J. Compos. Sci. 7 (5), 204. https://doi.org/10.3390/jcs7050204 (2023).
- 23. Hichem, R. & Bouhelal, S. Effect of the chemical modification of diatomite/isotactic polypropylene composite on the rheological, morphological and mechanical properties. *Adv. Mat. Res.* 1177, 121–136 (2023).
- 24. Zglobicka, I. et al. Poly (lactic acid) matrix reinforced with diatomaceous Earth. Materials 15 (18), 6210 (2022).
- 25. Dobrosielska, M. et al. Influence of diatomaceous Earth particle size on mechanical properties of pla/diatomaceous Earth composites. *Materials* 15 (10), 3607. https://doi.org/10.3390/ma15103607 (2022).
- Safaei, M. & Moghadam, A. Optimization of the synthesis of novel alginate-manganese oxide Bionanocomposite by Taguchi design as antimicrobial dental impression material. *Mater. Today Commun.* 31 https://doi.org/10.1016/j.mtcomm.2022.103698 (2022)
- 27. Malekhoseini, Z. et al. Effect of zinc oxide nanoparticles on physical and antimicrobial properties of resin-modified glass ionomer cement. *Dent. Res. J. (Isfahan).* **18** (1), 73 (2021).
- 28. Greessan, R., Jegan, J., Kannaki, S., Dineshkumar, S. & Kayalvizhi, A. Investigations on ZnO reinforced composite materials for electronic applications–a review. *Mater. Today Proc.* 74, 57–59 (2023).
- Shin, G. Y. et al. Effect of zinc oxide nanoparticle types on the structural, mechanical and antibacterial properties of carrageenan-based composite films. Food Sci. Preservation. 31 (1), 126–137. https://doi.org/10.11002/fsp.2024.31.1.126 (2024).
- 30. Chen, J. et al. The nano antibacterial composite film carboxymethyl chitosan/gelatin/nano ZnO improves the mechanical strength of food packaging. *Int. J. Biol. Macromol.* **220**, 462–471. https://doi.org/10.1016/j.ijbiomac.2022.08.005 (2022).
- 31. Moradpoor, H. et al. An overview of recent progress in dental applications of zinc oxide nanoparticles. RSC Adv. 11 (34), 21189–21206. https://doi.org/10.1039/d0ra10789a (2021).
- 32. Lin, M. H. et al. Hybrid zno/chitosan antimicrobial coatings with enhanced mechanical and bioactive properties for titanium implants. *Carbohydr. Polym.* 257, 117639. https://doi.org/10.1016/j.carbpol.2021.117639 (2021).
- 33. Zhang, W. & Xiong, R. Zinc oxide nanoparticles: synthesis, antibacterial activity and mechanism, *Nanomaterials*, vol. 6, no. 2, p. 20, (2016).
- 34. Bokobza, L. Elastomer nanocomposites: effect of filler-matrix and filler-filler interactions. Polym. (Basel). 15 (13), 2900 (2023).
- 35. Mandal, S. K., Kumar, R., Pradhan, A. R., Kumar, D. & Kumar, S. Impact of nano fillers on the mechanical and rheological behaviour of polydimethylsiloxane based nanocomposite elastomer. *Ceram. Int.* 51 (2025).
- 36. Litvinov, V. M., Orza, R. A., Kluppel, M., Van Duin, M. & Magusin, P. Rubber-filler interactions and network structure in relation to stress-strain behavior of vulcanized, carbon black filled EPDM. *Macromolecules* 44 (12), 4887–4900 (2011).
- 37. Hafezeqoran, A., Rahbar, M., Koodaryan, R. & Molaei, T. Comparing the Dimensional Accuracy of Casts Obtained from Two Types of Silicone Impression Materials in Different Impression Techniques and Frequent Times of Cast Preparation, *Int J Dent*, vol. 2021, [Online]. (2021). Available: https://api.semanticscholar.org/CorpusID:238354742
- 38. Tsai, W. T., Lai, C. W. & Hsien, K. J. Characterization and adsorption properties of diatomaceous earth modified by hydrofluoric acid etching., *J Colloid Interface Sci*, vol. 297 2, pp. 749–754, [Online]. (2006). Available: https://api.semanticscholar.org/CorpusID
- 39. Bello, O. S., Adegoke, K. A. & Oyewole, R. O. Insights into the Adsorption of Heavy Metals from Wastewater using Diatomaceous Earth, Sep Sci Technol, vol. 49, pp. 1787–1806, [Online]. (2014). Available: https://api.semanticscholar.org/CorpusID:97796439
- 40. Perera, H. J., Goyal, A., Banu, H. & Alhassan, S. M. Enhanced oil-spill removal and recovery from water bodies using diatomaceous earth and C18-silane-grafted polyurethane, *Emergent Mater*, vol. 6, pp. 499–509, [Online]. (2022). Available: https://api.semanticscholar.org/CorpusID:254485224
- 41. Klingshirn, C. F., Waag, A., Hoffmann, A. & Geurts, J. Zinc oxide: from fundamental properties towards novel applications, (2010).
- 42. Vikram, S. & Chander, N. G. Effect of zinc oxide nanoparticles on the flexural strength of polymethylmethacrylate denture base resin. Eur. Oral Res. 54 (1), 31–35. https://doi.org/10.26650/eor.20200063 (2020).
- 43. Donovan, T. E. & Chee, W. W. L. A review of contemporary impression materials and techniques, (2004). https://doi.org/10.1016/j.cden.2003.12.014
- 44. Ibraheem, R. O. Rheological properties of resin composite [Review Article]. *Biomaterials J.* 1 (1), pp13–17 (2022). https://biomatj.com/ojs/index.php/main/article/view/5 Accessed: Feb. 10, 2023. [Online]. Available:
- 45. Goldberg, A. J. Viscoelastic properties of silicone, polysulfide and polyether impression materials, *J Dent Res*, vol. 53, no. Spec., pp. 1033–1039, (1974).
- Aslan, Y. U. & Özkan, Y. K. Impression Material Selection According to the Impression Technique, Complete Denture Prosthodontics: Planning and Decision-Making, pp. 111–132, (2018). https://doi.org/10.1007/978-3-319-69032-2\_4
- 47. Majid, M., Hassan, E. D., Davoud, A. & Saman, M. A study on the effect of nano-ZnO on rheological and dynamic mechanical properties of polypropylene: experiments and models. *Compos. B Eng.* 42 (7), 2038–2046 (2011).
- 48. Blackburn, S. Influence of Powder Morphology on Paste Flow, [Online]. (2020). Available: https://api.semanticscholar.org/Corpus ID:224880999
- 49. Alkurt, M., Duymus, Z. Y. & Dedeoglu, N. Investigation of the effects of storage time on the dimensional accuracy of impression materials using cone beam computed tomography. *J. Adv. Prosthodont.* **8** (5), 380–387 (2016).
- Chai, N. et al. Isotropic sintering shrinkage of 3D glass-ceramic nanolattices: backbone preforming and mechanical enhancement, International Journal of Extreme Manufacturing, vol. 6, [Online]. (2023). Available: https://api.semanticscholar.org/CorpusID:266 507459

- 51. Garg, R. & Garg, R. Effect of zinc oxide nanoparticles on mechanical properties of silica fume-based cement composites. *Mater. Today Proc.* 43, 778–783 (2021).
- 52. Ariati, R., Sales, F., Souza, A., Lima, R. A. & Ribeiro, J. Polydimethylsiloxane composites characterization and its applications: A review. *Polym. (Basel).* 13 (23), 4258 (2021).
- 53. Abdalqadir, M., Faraj, S. & Azhdar, B. An evaluation of a technique to improve the mechanical properties of maxillofacial silicone elastomers with zinc oxide nanoparticles. *J. Prosthet. Dent.* 128 (3), 531–538 (2022).
- Sales, F. C. P., Ariati, R. M., Noronha, V. T. & Ribeiro, J. E. Mechanical characterization of PDMS with different mixing ratios. *Procedia Struct. Integr.* 37, 383–388 (2022).
- Cordeiro, G. & dos Santos, A. A. M. Correlating diatomite particle characteristics with the rheology of fresh Cement-Based pastes. Available SSRN 4234536 (2022).
- Hassan, Y. M. et al. The influence of ZnO/SiO2 nanocomposite concentration on rheology, interfacial tension, and wettability for enhanced oil recovery. Chem. Eng. Res. Des. 179, 452–461 (2022).
- 57. Cevik, P. Evaluation of shore A hardness of maxillofacial silicones: the effect of dark storage and nanoparticles. Eur. Oral Res. 52 (2), 99–104 (2018).
- 58. Savin, C., Antohe, M. E., Balan, A., Sirghe, A. & Gavrila, L. Study regarding the elastic impression biomaterials dimensional stability. *Rev. Chim. (Bucharest)*. **70**, 797–800 (2019).
- 59. Mohammed, A. J. & Alirhayim, R. N. The effect of nanoparticles addition on the physical properties of the maxillofacial silicone: A literature review. *J. Biomater. Nanobiotechnol.* **10**, 11–23 (2019).
- 60. Masyuk, A., Katruk, D. & Levytskyi, V. Polylactide composites with calcium-containing fillers.
- 61. Ghannam, H., Chahboun, A. & Turmine, M. Wettability of zinc oxide Nanorod surfaces. RSC Adv. 9 (65), 38289-38297 (2019).
- 62. Zaid, H. M., Adil, M., Chuan, L. K. & Latiff, N. R. A. Stability and electrorheology of ZnO nanofluids in the presence of anionic surfactants, in *AIP Conference Proceedings*, AIP Publishing, (2016).
- 63. Qulub, F. & Wardhani, İ. F. Effect of Hydroxyapatite Filler on Mechanical Properties of PE/HAp Composite as a Candidate for Bone Repair, *Indonesian Applied Physics Letters*, [Online]. (2023). Available: https://api.semanticscholar.org/CorpusID:266269968
- 64. Mustapha, K., Ayinla, R. O., Ottan, A. S. & Owoseni, T. A. Mechanical properties of calcium carbonate/eggshell particle filled polypropylene Composites, *MRS Adv*, vol. 5, pp. 2783–2792, [Online]. (2020). Available: https://api.semanticscholar.org/CorpusI D:225493286
- 65. Mohammadi, Z. & Shahrabi, T. Antibacterial evaluation of zinc oxide Eugenol cement. Iran. Endod J. 9 (4), 243-247 (2014).
- Moezzi, A., McDonagh, A. M. & Cortie, M. B. Zinc oxide particles: synthesis, properties and applications. Chem. Eng. J. 185–186. https://doi.org/10.1016/j.cej.2012.01.076 (2012).
- 67. Shid-Moosavi, T. S., Mohammadi, N., Gharamani, Y., Motamedifar, M. & Alizadeh, A. A. Evaluating antimicrobial activity and cytotoxicity of silver nanoparticles incorporated into reinforced zinc oxide eugenol: an in vitro study. *Eur. Archives Pediatr. Dentistry.* 25 (3), 443–450. https://doi.org/10.1007/s40368-024-00905-7 (2024).

# **Acknowledgements**

Not applicable.

#### **Author contributions**

SH contributed to the conception and design of the study, interpretation of the analyzed data, data checking and validation, and critical review of the manuscript. MF contributed to the conception and design of the study, data collection, interpretation of the analyzed data, data checking and validation, and writing of the manuscript and critically reviewed the manuscript. NN & MG contributed to the conception and design of the study and data collection. All the authors read and approved the final manuscript.

#### **Funding**

Not applicable.

# **Declarations**

# Competing interests

The authors declare no competing interests.

# Ethical approval

Not applicable.

#### Additional information

Correspondence and requests for materials should be addressed to S.H.

Reprints and permissions information is available at www.nature.com/reprints.

**Publisher's note** Springer Nature remains neutral with regard to jurisdictional claims in published maps and institutional affiliations.

Open Access This article is licensed under a Creative Commons Attribution-NonCommercial-NoDerivatives 4.0 International License, which permits any non-commercial use, sharing, distribution and reproduction in any medium or format, as long as you give appropriate credit to the original author(s) and the source, provide a link to the Creative Commons licence, and indicate if you modified the licensed material. You do not have permission under this licence to share adapted material derived from this article or parts of it. The images or other third party material in this article are included in the article's Creative Commons licence, unless indicated otherwise in a credit line to the material. If material is not included in the article's Creative Commons licence and your intended use is not permitted by statutory regulation or exceeds the permitted use, you will need to obtain permission directly from the copyright holder. To view a copy of this licence, visit <a href="https://creativecommons.org/licenses/by-nc-nd/4.0/">https://creativecommons.org/licenses/by-nc-nd/4.0/</a>.

© The Author(s) 2025